



Shape Optimization and Sensitivity Analysis of a Morphing-Wing Aircraft

Cheng Gong¹ · Bao-Feng Ma¹

Received: 28 November 2017 / Revised: 21 September 2018 / Accepted: 1 October 2018 / Published online: 2 January 2019
© The Korean Society for Aeronautical & Space Sciences and Springer Nature Singapore Pte Ltd. 2019

Abstract

Morphing-wing concepts have received growing interests in the recent years for enhancing the multi-mission performance of unmanned aerial vehicle. However, to obtain a feasible morphing strategy, the optimization design studies are required. In this paper, an aerodynamic optimization study for a morphing-wing aircraft with variable sweep, span, and chord length was conducted to obtain the optimum configurations at subsonic, transonic and supersonic conditions. The optimization objective is to obtain maximum lift-to-drag ratios subject to lift coefficients and static stability constraints at each flight condition. A genetic algorithm in conjunction with surrogate models was employed to search optimum solutions in the entire design space. The aerodynamic forces are calculated by an Euler-based solver and friction drag estimation code. The optimum configuration corresponding to any flight condition can be determined through the optimization. A global sensitivity analysis based on the surrogate model was also carried out, hence the contribution of each design variable to the optimization objective can be analyzed. The results indicated that the optimum wing at subsonic speeds have a lower sweep angle and high aspect ratio, and the wing sweep has a primary contribution to lift-to-drag ratios, and the span is secondary; at transonic conditions, the medium-sweep wing is the optimum, and the contribution of the span is far more than other variables; at supersonic conditions, the optimum configuration becomes a high-sweep cropped delta wing, and the span has a dominant contribution, and the sweep is secondary.

Keywords Morphing aircraft · Aerodynamic optimization · Global sensitivity analysis

1 Introduction

Morphing aircraft is able to effectively compromise the conflicts between various design requirements by significantly changing the shape, compared to fixed-geometry aircraft. Morphing aircraft is not a new concept [1], and some early flight vehicles with variable sweep, as one type of morphing aircraft, have been developed and produced, such as the Soviet Union MIG-23, the United States F-14, and the European Tornado. The motivation of the variable-sweep designs comes from multi-mission requirements of aircraft in the 1950s and 1960s. For this purpose, larger wings would be required for fulfilling the strict multipoint mission objectives if a fixed-wing design was employed; as a result, the fixed-wing aircraft would be heavier than their morphing-

wing counterparts, as reviewed by Weisshaar [1]. Therefore, in the context of multi-missions, the variable-sweep wing is superior to the fixed-wing. Similarly, with disappearance of the demand for multi-missions subsequently, the variable-sweep aircraft become unpopular gradually, because, for a single-mission aircraft, the variable-sweep design imposes considerable penalties in weight due to relatively complex control mechanisms for changing the geometries. Nevertheless, from 1990s, with development of unmanned aerial vehicles (UAVs) that are commonly required with multi-mission capacities, morphing aircraft concepts have raised a renewed interest.

The wings have a key role in the aerodynamic characteristics of aircraft as main aerodynamic components; therefore the shape-morphing aircraft mainly changes the wing shape to increase the performance. Although arbitrarily morphing the wing geometry is the most ideal situation, a more efficient and feasible manner is only changing the key parameters of the wing, such as airfoil profiles, sweep angles, and wing span. Multidisciplinary efforts [2] are required to develop

✉ Bao-Feng Ma
bf-ma@buaa.edu.cn

¹ Ministry-of-Education Key Laboratory of Fluid Mechanics, Beihang University, Beijing 100191, China

the morphing aircraft, in which aerodynamic optimization is an important tool in seeking optimum configurations for each flight condition. Aerodynamic shape optimization for a morphing wing is considerably different from conventional fixed-wings [3]. For the fixed-wing aircraft, the optimization design is conducted around a baseline configuration with smaller geometric alteration [4–9], but for the morphing aircraft, larger deformations are required in optimization. In addition, the optimum configurations are necessarily selected from the shape set being capable to be obtained by the driving mechanisms of the morphing [10].

In industry fields, the Defense Advanced Research Projects Agency in the United States was contracted to three companies to develop morphing aircraft concepts [1]. The Lockheed Martin Company proposed a folding-wing concept. The Raytheon company proposed an unswept variable-span concept for multi-mission cruise missiles, and the evaluation on the strategy indicated that the design can increase 75% more loiter time at the end of flight. NextGen Aeronautics Corporation designed a sliding-skin aircraft, the wing of which moves between five different wing planforms and changes planform in area, span, chord, and sweep. Although all three designs satisfied the technical targets, only the Lockheed Martin and the NextGen schemes were chosen for wind tunnel testing. Eventually, only the sliding-skin wing design by NextGen Aeronautics Corporation was selected for building a sub-scaled demonstrator MFX2. Therefore, from the perspective of engineering, morphing the variable sweep, span, and chord length together is a feasible and preferable morphing strategy. The present study will focus on this kind of morphing manner.

In academic communities, existing studies on the aerodynamic optimization of morphing aircraft consist of airfoil morphing [10–13] and wing planform morphing [13–21]. The wing planform has several parameters to change, e.g., sweep angle [14], span [15–18], wing twisting [19, 20], wing flexibility [21], among which the sweep angle, chord length and span are three key parameters that can significantly influence the aerodynamic characteristics of aircraft at various flight conditions. Gamboa et al. [13] studied the optimization of a morphing aircraft with variable span and chord length using panel and nonlinear lifting-line methods. Bae et al. [15] calculated static and dynamic aeroelasticity for UAV with variable span. Mestrinho et al. [16] studied the design optimization of a small variable-span morphing UAV. Ajaj et al. [17], and Woods and Friswell [18] proposed a new strategy for variable-span aircraft, and evaluated the benefits in enhancement of aerodynamic characteristics and flight control. It can be anticipated that the performance of morphing vehicles could be improved if the sweep, chord length and span are changed together, but the associated investigations are absent and the effects of design variables on the aerodynamic characteristics are also worth study-

ing further. More importantly, these existing optimization studies for morphing airfoils and wing planforms, basically adopted low fidelity methods, such as panel or vortex lattice methods, for the calculation of aerodynamic forces in optimization. Up to date, very few aerodynamic optimizations for morphing aircraft adopted high fidelity computational fluid dynamics (CFD) methods. Although the wing twist morphing has been investigated using a CFD method [19], aerodynamic optimization for large-deformation morphing aircraft like variable sweep, span, and chord length in a broad range of variable values was not reported up to date.

The present investigation aims to study the combined effects of sweep, root chord length and span on the aerodynamic characteristics of a generic morphing-wing aircraft using an optimization process based on CFD solvers, which has never been reported in previous studies. Each geometric design variable will be changed in a wide range of values, so the morphing is involved in large deformations. The large deformations pose a challenge to CFD-based optimization, in which mesh deformation approaches that are commonly employed in conventional optimization is ineffective, convenient and efficient mesh redrawing methods are necessary. In our study, a Cartesian grid approach was applied to morphing-wing optimization, by which the problem for large deformation can be easily solved through mesh rebuilding. Although the current state-of-the-art method for CFD-based optimization is based on Navier–Stokes equations, the Euler-based approach is still employed extensively due to its higher computational efficiency [6–8]. The parameters being modified at flight, such as sweep angle, span, chord length, and angle of attack, will be chosen as the design variables for optimization. Although other parameters, e.g., wing twist, also have an effect on aerodynamic characteristics of aircraft, they do not belong to the morphing parameters in the present case. The type of non-morphing parameters can be optimized using conventional optimization methods after the optimum sweep and span have been determined, which is not the focus of interest in the present study. The optimum configurations will be determined at subsonic, transonic, and supersonic conditions. It should be noted that conventional aerodynamic optimization is commonly based on a reference configuration, but the morphing aircraft will tailor their configurations to an optimum one at each flight condition, therefore no reference configurations exist. Besides the optimization study, a global sensitivity analysis is also applied to analyze the effects of the associated design variables on aerodynamic characteristics, which can identify the most sensitive one from design variables. Since three design variables are changed simultaneously in optimization, the contribution of each variable is quite difficult to determine only based on the knowledge of classic aerodynamics. In addition, although importance of aeroelastic characteristics is raised in design-

ing a morphing aircraft [13, 15, 19], it is not involved in the present study.

2 Physical Model and Surrogate Methodology

2.1 Problem Description

The morphing aircraft is designed as a small UAV with variable sweep, root chord length and span, as shown Fig. 1, which is a wing–body–tail configuration. The root chord length (c_{root}), sweep angle (λ), and span (s) of the wing can be changed. However, the structure detail of driving the morphing of aircraft is not involved in the present investigation, and it is assumed that the shape deformation can be implemented by a sliding-skin mechanism like the demonstrator MFX2. The sweep angle is altered with a shearing manner, in which the airfoil can always be aligned with an incoming stream as the wing varying. The airfoil of

the wing has a maximum thickness of 4.6% chord length. The wings are located 0.07 m high above the horizontal symmetry plane of the fuselage. The fuselage is an axisymmetric ogive-cylinder body, and the vertical and horizontal tails are sweep wings with a maximum thickness of 6% chord length. The horizontal tails are located 0.07 m low below the horizontal symmetry plane of the fuselage.

The aerodynamic optimization aims to maximize the lift-to-drag ratio subject to the constraints on lift coefficients and static stability at subsonic, transonic and supersonic flight conditions (Table 1), in which different flight speeds correspond to different altitudes (H). The flight altitude can influence incoming Reynolds numbers that will be considered in estimating skin-friction drag. The design variables consist of sweep angle, root chord length, span, and angle of attack, as shown in Table 2. For any optimization design, constraints conditions are required to obtain practical optimization results. Herein the static stability and lift coefficients are constrained at various flight conditions, both of which is assumed to be able to change in a narrow range

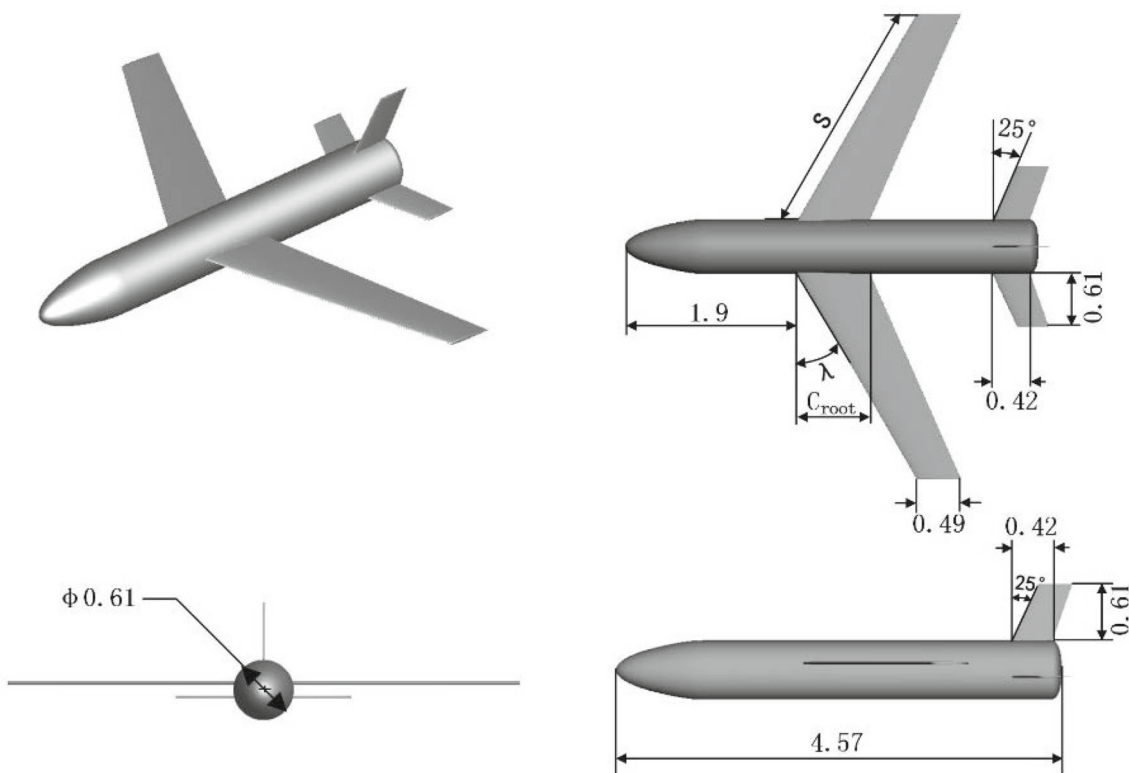


Fig. 1 Morphing-wing aircraft, in meter

Table 1 Three flight conditions

Cases	Mach	H/m	$W \times 10^{-3}/kg$	C_L	c.g. (m)	$\partial C_M / \partial C_L$
1	0.5	20	1.5–2.0	0.47–0.58	1.94	(– 0.06, – 0.04)
2	0.85	5000	1.5–2.0	0.30–0.38	2.33	(– 0.06, – 0.04)
3	2.0	300	1.5–2.0	0.030–0.038	2.79	(– 0.06, – 0.04)

Table 2 Optimization problem setup

Objective function/variables/constraints	
Maximize	
C_L/C_D	Lift-to-drag ratio
With respect to	
α	Angle of attack
λ	Sweep angle
s	Span
c_{root}	Root chord length
Subject to	
C_L	Lift coefficient constraint
$\partial C_M/\partial C_L$	Static stability constraint

due to uncertainties of aircraft weight in flight. The center of gravity (c.g., distance from the body nose tip) should vary with the morphing in terms of design experience of existing variable-sweep aircraft.

With increasing sweep angle, the aerodynamic center of the aircraft can be significantly moved backward, particularly at supersonic speeds, which can cause the aircraft to be strongly stable, thus leading to larger trim drag and being difficult to control in pitch. Therefore, static stability margin is necessarily designed in a reasonable range for maintaining a good stability performance. To fulfill this requirement, variable-sweep aircrafts (e.g., F-14 Tomcat) are commonly required to artificially move c.g. through pumping fuel forward and backward in equilibrium fuel tanks, which can be easily implemented by automatic control of computers. Herein the c.g. in each optimization condition was taken as a given design parameter (see Table 1). The static stability in pitch ($\partial C_M/\partial C_L$) is also an important constraint in optimization, which was evaluated using a second-order centered difference scheme $(C_M^{\alpha_0+\Delta\alpha} - C_M^{\alpha_0-\Delta\alpha})/(C_L^{\alpha_0+\Delta\alpha} - C_L^{\alpha_0-\Delta\alpha})$. Herein we did not constrain the pitching moment, because it can be trimmed by pitching elevators after optimization.

Although there are only four design variables, each variable will be discretized into a series of sampling points to construct surrogate models. Owing to the wider variable bounds, too few sampling points are unable to capture the details of the surrogate models. To fulfill the accuracy of the model, new data points need to be added in the sampling process. Eventually, a total of 144, 324, and 180 samples are calculated for subsonic, transonic, and supersonic cases. Additionally, the static stability constraint was computed using a second-order centered differencing scheme, so each sample needs three data to obtain the differencing. Therefore, CFD calculations need to be invoked for 432, 972, and 540 times for three flight speeds, and each flight condition is computed with 1.6 million (subsonic), 1.9 million (tran-

sonic), and 1.4 million (supersonic) grid cells. In this case, it is not necessary to conduct the direct genetic algorithm (GA) optimization. The GA optimization is extremely time-consuming for 3D shape optimization, and mainly applied on 2D optimization as yet. In addition, for the direct GA in conventional fixed-wing optimization, it is typically not necessary for obtaining the real minimum (or maximum) values, and it will be acceptable as long as the sub-optimum values are some amount better than a baseline configuration. However, for the present morphing aircraft, no baseline configuration exists. If let the GA fully converges to obtain the same accuracy with the surrogate method, it is completely not affordable for 3D geometries.

2.2 Optimization Framework

2.2.1 Surrogate Model

The whole optimization process is integrated using a platform program with a graphic interface coded by MATLABTM language. The optimization process is based on surrogate models, which is computationally efficient and robust and has been applied extensively in aircraft optimization design [22, 23]. Two models were employed, including the polynomial response surfaces (RSM) and Kriging model. The current optimization study for the morphing aircraft involved large-scale variable sweep, chord length and span; hence it is difficult to guarantee that there is necessarily a single local minimum in the design space, and a global optimization algorithm (e.g., genetic algorithm) is necessarily employed rather than a local gradient algorithm. However, the global algorithms based on CFD computations are extremely time-consuming and affordable, and existing optimization studies for CFD-based optimization computations basically adopt local algorithms. To avoid the high computational cost in the global optimization, a surrogate model is employed in the present study, and the global optimization is conducted on the surrogate model. In constructing the surrogate models, design of experiments based on full factor analysis is first performed to obtain reasonable distributions of design variables. The third-order response surface and common Kriging models were employed, and the optimizer for the surrogate models is based on a genetic algorithm. To choose a suitable order number of the response surfaces, we first tried a second-order response surface, and found that it is not enough to represent the sample data. Then, the third-order response model was tested, accuracy of which is sufficient for fitting the sample data, therefore the fourth-order response model is not necessary. The fitting accuracies for the third-order response model will be presented in Results.

2.2.2 Geometric Parameterization, Grid Generation, and CFD Solver

The geometric parameterization is implemented using an open source code OpenVSP that is a conceptual design tool for aircraft [24]. The model in OpenVSP is divided into various components, such as wing, body, horizontal tails, and vertical tails, and each component is parameterized separately. The current investigation only changes the wing shape, and the wing is parameterized by planform parameters, e.g., span, chord and sweep, etc. The wing parameters can be modified by hooking OpenVSP API functions that can be accessed through a C-like language script (Angelscript). By coding the script program, the design variables for the wing can be modified. The model can be natively created in OpenVSP, or generated using other modeling software and then be inputted into the OpenVSP and then re-parameterized [25].

The CFD solver for computing aerodynamic coefficients during the optimization is an inviscid Euler solver Ansys Cart3d (a commercial version of the Cart3d developed by Aftosmis [26, 27]), and in the optimization process, the CFD solver is called repeatedly to obtain aerodynamic force coefficients. The solver is based on octree-based Cartesian grids and a finite volume method. The original version of Cart3D has been extensively employed in conceptual design of aircraft recently [28, 29]. Comparing with viscous CFD solvers based on Navier–Stokes equations, Euler solvers are much more efficient, thus are being extensively applied in aerodynamic optimizations [6, 7]. In a process of aircraft design, various fidelity models for aerodynamic optimization are required to satisfy the requirements in different design phases. The choice for the computational tools depends on a tradeoff in efficiency and accuracy. Cartesian volume meshes required by Cart3D can be generated automatically based on watertight surface meshes with triangularization; the surface grids were generated using a triangularization algorithm based on the parameterized models in OpenVSP. Grid cells inside the model will be removed, and the volume cells intersected with the surface grids will be cut by the triangular surface meshes. Therefore, the cut-cells near the surface are irregularly polyhedral, but not necessarily hexahedral. Entire computational domains are hexahedral for all cases; therefore the specific domain sizes vary with flight conditions varying. The surface meshes for each component of aircraft can be created individually, and an intersection program in the Cart3D tool set can be employed to implement a Boolean operation for these surface meshes, obtaining the watertight surface mesh. Fully intersected watertight surface triangulation can also be obtained using OpenVSP. In the present study, the intersection tool of Cart3D was used. The intersection operation of surface meshes and automatic generation of volume meshes are extremely important in the optimization of morphing aircraft with large deformations, which guarantees that

the large morphing such as variable sweep, chord length and span, can be implemented in the optimization. The second-order Van Leer scheme was selected for the flux computation, and the Van Leer limiter was added in a supersonic computation. The computation is steady and time-independent in which a pseudo time-marching method was used with a fifth-stage Runge–Kutta scheme and local time step. The wall is set as a slip boundary condition, and the outer boundary of the domain is set as a far field condition.

A friction/form drag estimation program was employed to calculate the friction/form drag, because the friction drag will be unable to be calculated based on inviscid Euler equations. The estimation of the friction drag adopts the method of Gur et al. [30] that can provide an estimate of laminar and turbulent skin friction and form drag for each component of an aircraft. The estimation method has been successfully applied to the high-fidelity shape optimization of aircraft in previous studies [8]. The friction drag for fuselage-like components is estimated separately from the wing-like components, and the total drag is the drag summation of all components. The formula of the estimation for each component is illustrated in the following (1), in which S_{wet} and S_{ref} are the wetted and reference area; C_F is a friction coefficient and FF is a form factor. C_F uses standard flat-plate skin-friction formulas, and the compressibility effects are included using the Eckert reference temperature method for laminar flow and the van Driest II formula for turbulent flow. A composite formula can be utilized to include the case of partially laminar and turbulent flow. Form factors (FF) are employed to estimate the effect of thickness on the drag, and the associated formulas for body of revolution and wing are shown in (2) and (3) in which d and l are the diameter and length of the body, and t and c are the thickness and chord length of the wing. The formula (1) is valid from subsonic to moderate supersonic speeds (about Mach 3)

$$C_{D,f} = C_F FF \frac{S_{\text{wet}}}{S_{\text{ref}}}, \quad (1)$$

$$FF_{\text{body}} = 1.0 + 1.5 \left(\frac{d}{l} \right)^{1.5} + 50 \left(\frac{d}{l} \right)^3, \quad (2)$$

$$FF_{\text{wing}} = 1.0 + 2.7 \left(\frac{t}{c} \right) + 100 \left(\frac{t}{c} \right)^4. \quad (3)$$

2.3 Global Sensitivity Analysis

The surrogate models can also be exploited to conduct a sensitivity analysis on these design variables except for the optimization. Herein a global sensitivity analysis method (Saltelli and Sobol [31]) was utilized to evaluate the impact level of the design variables on the optimization objectives, thus determining the most sensitive parameter of the wing. The global sensitivity analysis for design variables is a class of prob-

abilistic methods which characterize the input and output uncertainties as probability distributions, and decompose the output variance into the parts contributing to input variables and their combinations. Hence, the sensitivity of the output to input variables can be measured by the amount of variance in the output caused by that input. The analysis method can fully explore the input space with interactions, and nonlinear responses. For these reasons, the method is widely employed as it is feasible to calculate them [32, 33]. It should be noted that the full variance decomposition is only meaningful as the input factors is independent from one another.

3 Results and Discussion

In the section, the validation of the numerical approach was first demonstrated to evaluate the reliability of the optimization results. Subsequently, the optimization results for three cases with subsonic, transonic and supersonic conditions are presented. These three conditions are optimized independently and the optimum configuration for each condition is achieved, and the effects of design variables on the optimization objective are also analyzed.

3.1 Validation of Numerical Approach

The Cart3D code as a mature inviscid Euler solver has been verified and validated extensively [26]. Herein to validate the reliability of the hybrid method by combining the Euler solver and friction drag estimation used in the optimization, the simulations were conducted for two standard models, for which experimental data are available at transonic and supersonic speeds, and the results of validation are shown in Fig. 2. The following grids are all based a half model since no sideslip exists.

The aircraft model for validating the transonic computation is DLR-F6 model that can be found in the drag prediction

workshop website [34]. A grid convergence testing is first carried out to study the effects of grid discretization, the lift and drag coefficients start to be approximately unchanged as the grid amount is more than 0.6 million. Figure 2a shows a comparison with experimental data and other CFD results, and the experimental data have an accuracy of ± 0.0001 . The maximum error of drag at a specified lift coefficient is -7.4% that is almost the same magnitude with the error caused by Fluent code. However, Fluent code overestimates the results over the experimental values, but the present method underestimates the results, as expected. The transonic case is generally more difficult to simulate due to the mixed flows with subsonic and local supersonic speeds. Herein the good consistency is attributed to the lower angle of attack (AOAs) (less than 2°) at which experimental data can be expected to be available. At the lower AOAs, no significant flow separation exists around the model. Hence, the inviscid simulation can have a rather good performance in predicting drag except for friction drag. For our simulations, the cruise AOAs are designed below 5° for all flight conditions.

A supersonic aircraft model [35] was employed to validate the supersonic computation. Grid convergence testing was first conducted, and the supersonic computation is more prone to converge with increasing grid cells, and as the grid cells are more than 0.1 million, the results are basically unchanged, and have a good agreement with the experimental data. There is only a deviation of 4.3% in maximum with respect to the experimental values. It should be noted that the AOA for the maximum lift coefficient is 31.5° at the supersonic case, and at such high AOAs, the computational results are still extremely close to the experimental values. The reason is that the wave drag accounts for most of the total drag at a supersonic condition, which is able to be correctly captured by an inviscid solver.

Prior to a formal optimization, a grid convergence study for the present morphing aircraft was conducted at transonic and supersonic conditions to determine a suitable grid

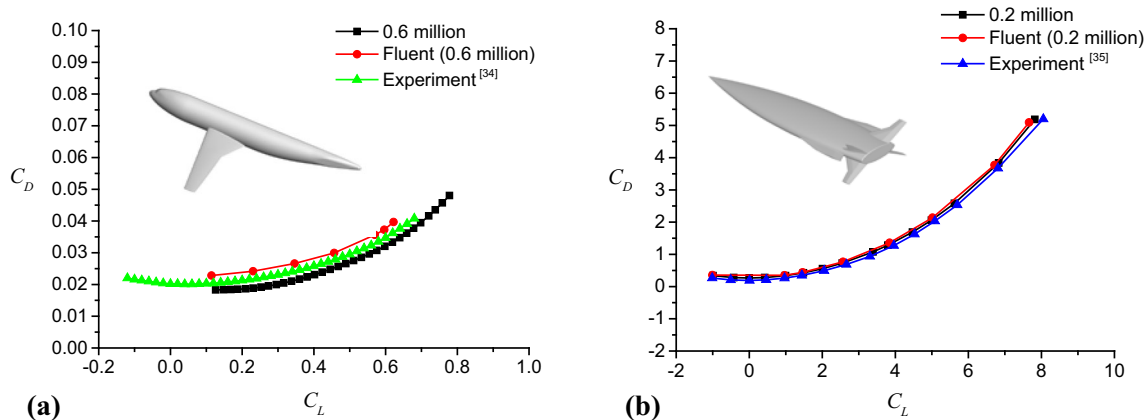


Fig. 2 Validation of numerical results. **a** DLR-F6 model at $Ma = 0.75$ [34]; **b** supersonic model at $Ma = 2.5$ [35]

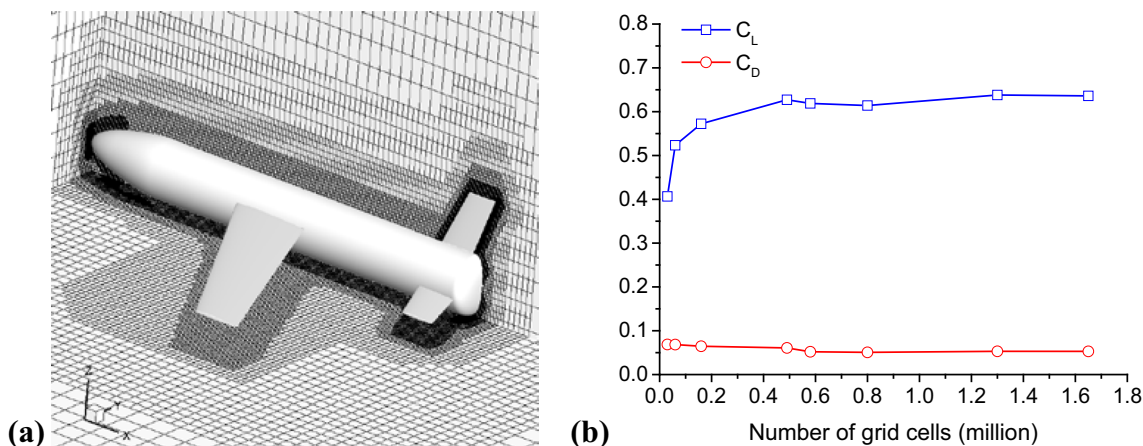


Fig. 3 Computational grids **a** and grid convergence validation **b** at a transonic condition

quantity for the optimization. The results indicated that the supersonic case can converge more quickly than the transonic one by increasing the grid amount, which is consistent with the results in Fig. 2. The lift and drag coefficients for one configuration with $\lambda = 30$ deg, $c_{root} = 0.8$ m, $s = 2.7$ m and $\alpha = 3.0^\circ$ at a transonic condition ($Ma = 0.85$) are shown in Fig. 3, in which the aerodynamic coefficients basically retain a minor variation after 0.6 million. Since hundreds of computations during the optimization will be performed for each case, the grid amount for various flight conditions is optimized in terms of the results of the grid convergence, by comprising computational efficiency and accuracy. The specific grid amounts and computational domain sizes will be shown in the next section with the optimization results for each flight condition.

3.2 Optimization Results

In this subsection, the optimum configurations for the morphing aircraft at subsonic, transonic and supersonic conditions are presented, and the parameter sensitivity of associated design variables was also analyzed by the global sensitivity analysis method, thus determining the contribution of each variable to the optimization objective.

3.2.1 $Ma_\infty = 0.5$ and $H = 20$ m

At the subsonic case, the searching range for design variables in optimization is shown in Table 3, in which the variable values are set in a relatively narrow range based on the results of a pre-optimization process with coarser variable intervals, which can increase computational efficiency in optimization. The computational domain is a hexahedron of 20 times body length upstream of the nose tip, 20 times body length downstream of the bottom end of the fuselage, and 20 times body length at

Table 3 Range of design variables at $Ma_\infty = 0.5$

Design variables	α/deg	c_{root}	λ/deg	s/m
Lower bound	1.0	0.49	0.0	2.3
Upper bound	5.0	0.64	10.0	2.7

Table 4 Optimization results at $Ma_\infty = 0.5$

Models	α/deg	c_{root}	λ/deg	s/m	C_L	$\partial C_M/\partial C_L$	C_L/C_D
RSM	3.4	0.55	2.7	2.7	0.54	-0.06	11.6
Kriging	3.1	0.54	2.7	2.7	0.47	-0.06	11.6

the side from a symmetry plane. Total grid cells are around 1.6 million that can vary slightly with re-meshing the geometry during the optimization. The grid amount is sufficient in terms of the preceding grid convergence testing.

Based on the sampling points, the CFD solver and friction drag estimation code are invoked to calculate aerodynamic force coefficients, eventually obtaining the surrogate models of the lift-to-drag ratio. To validate the fitting accuracy of the surrogate models, ten additional random sampling points, not belonging to the original ones, were added to obtain additional aerodynamic coefficients using the computational module. By comparing the fitting values of the surrogate models, the fitting accuracy was estimated with a R^2 value of 0.99. The R^2 is a traditional index for evaluating the fitting reliability with a range of 0–1, and a higher R^2 value indicates that the fitting accuracy is good.

A global optimization algorithm (genetic algorithm) was carried out on the surrogate models, and the optimization result is shown in Table 4 in which the optimum parameters are similar for RSM and Kriging models with minor differences. It is known that a wing with low-sweep and high aspect ratio have better aerodynamic characteristics at sub-

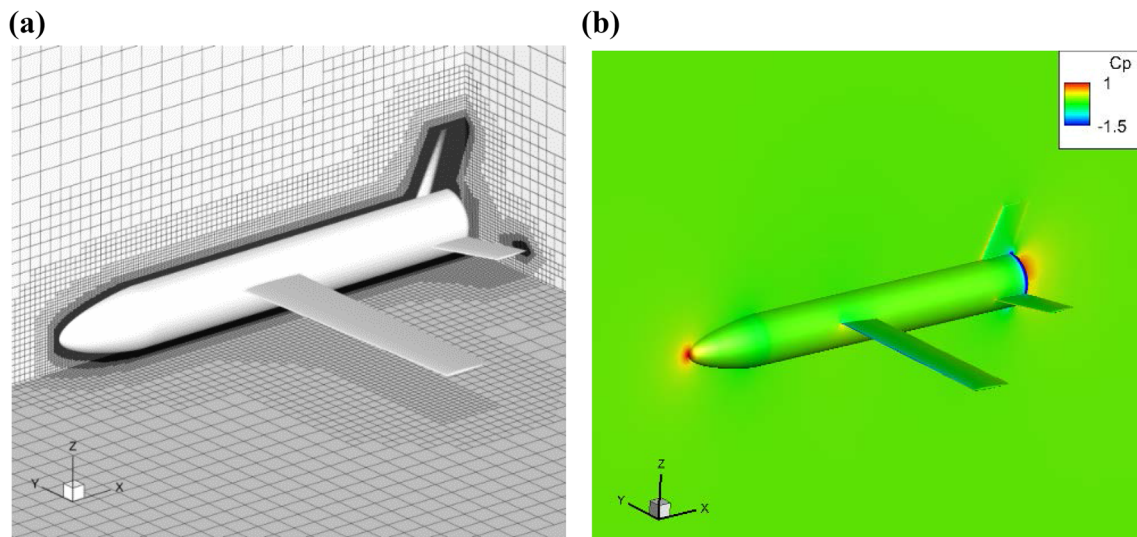


Fig. 4 Optimum configuration at $Ma = 0.5$. **a** Optimum configuration and grid; **b** pressure field

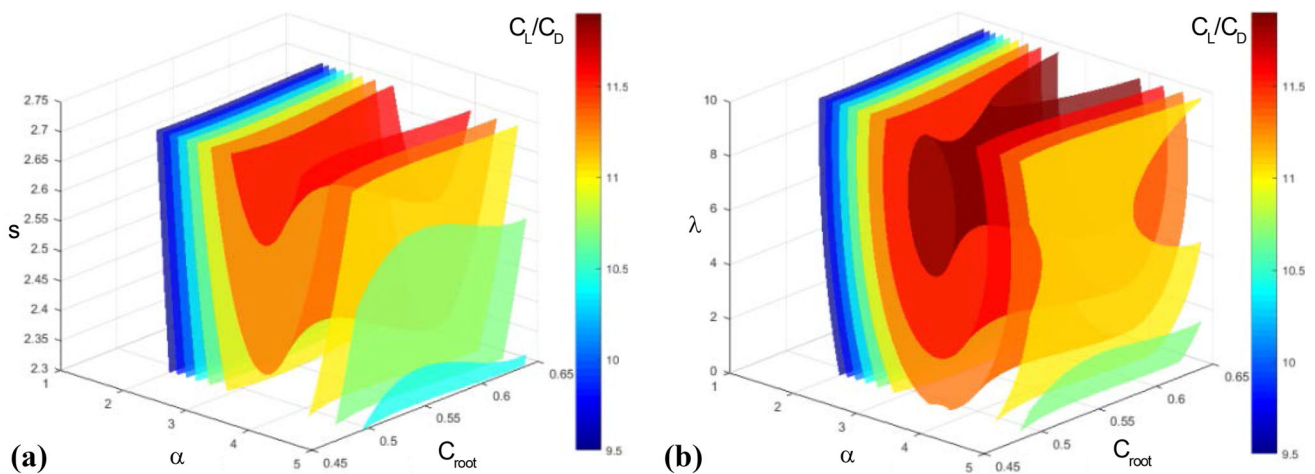


Fig. 5 Iso-surfaces of response surface at $Ma = 0.5$. **a** C_L/C_D v.s. α , c_{root} and s with $\lambda = 3.2$ deg; **b** C_L/C_D v.s. α , c_{root} , and λ with $s = 2.7$ m

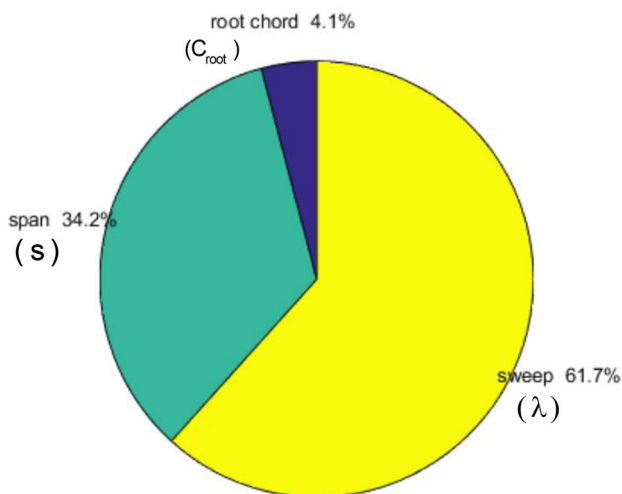


Fig. 6 Global sensitivity results of design variables at $Ma = 0.5$

sonic speeds, therefore the optimum parameters with 2.7° sweep angle and full span (2.7 m) in Table 4 is reasonable even identified by common experience. The optimum configuration also satisfies static stability and lift coefficient constraints. Figure 4 shows the optimal configuration with the associated computational grid, and the corresponding pressure contour is also presented, which is a typical subsonic flow field.

The iso-surfaces with one variable being constant are illustrated in Fig. 5 for demonstrating the surrogate models (RSM). It can be seen that the lift-to-drag ratio C_L/C_D exhibits a maximum with increasing angle of attack (Fig. 4a, b), and the span (Fig. 5a) and sweep angle (Fig. 5b) have significant effects on the optimization objective near the optimum solution, whereas the root chord length has a relatively small impact (Fig. 5a, b). The contribution of each geometric design variable to the lift-to-drag ratios is displayed with

Table 5 Range of design variables at $Ma_\infty = 0.85$

Design variables	α/deg	C_{root}	λ/deg	s/m
Lower bound	0.6	0.5	10.0	1.7
Upper bound	4.0	0.7	40.0	2.3

Table 6 Optimization results at $Ma_\infty = 0.85$

Models	α/deg	C_{root}	λ/deg	s/m	C_L	$\partial C_M/\partial C_L$	C_L/C_D
RSM	3.0	0.59	28.2	1.97	0.38	-0.06	7.18
Kriging	3.1	0.57	28.4	1.97	0.38	-0.06	7.35

a percentage in Fig. 6 based on the parameter sensitivity analysis. The wing sweep has a primary contribution to the lift-to-drag ratios, and the span is secondary, and the root chord length has a minimum impact.

3.2.2 $Ma_\infty = 0.85$ and $H = 5000$ m

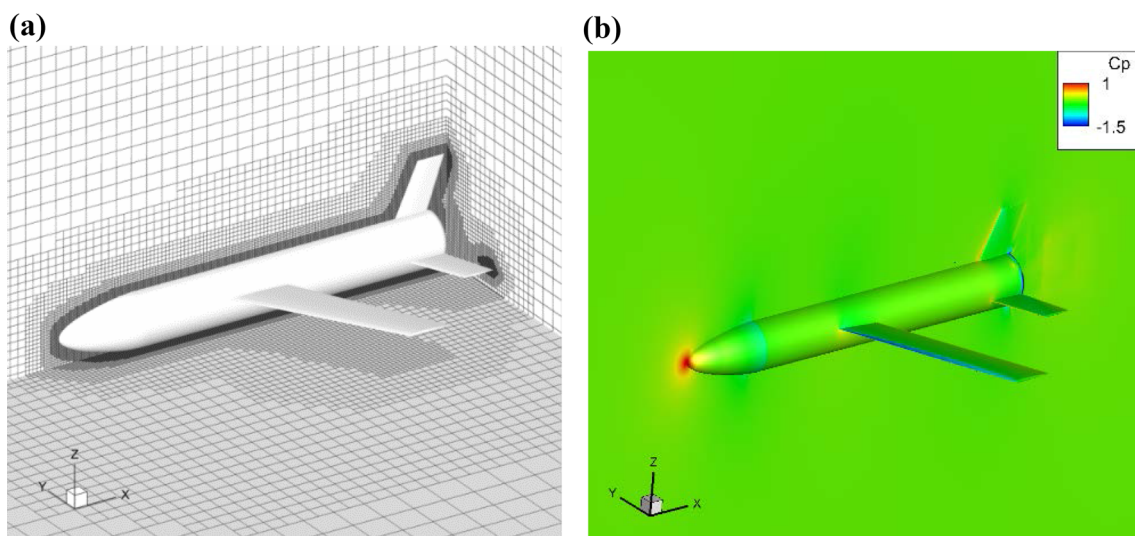
At the transonic case, the range of design variables is shown in Table 5 in terms of a pre-optimization result. The computational domain is the same size with the preceding subsonic case. Total grid cells are around 1.9 million which is higher than the subsonic case, and will vary slightly with the re-meshing during the optimization. The grid amount is sufficient in terms of the preceding grid convergence testing. The surrogate models at this case based on 324 data points are employed, which is obtained by invoking the CFD solver and friction drag estimation code repeatedly. The fitting accuracy of the surrogate models was estimated with a R^2 value of 0.98, indicating that the fitting accuracy is good.

The optimization result is shown in Table 6, in which the optimum parameters are similar for RSM and Kriging models with minor differences. The wing with a medium-sweep angle and aspect ratio has better aerodynamic characteristics at transonic speeds. The optimum configuration also satisfies static stability and lift coefficient constraints. Figure 7 shows the optimal configuration with the associated computational grid, and the corresponding pressure contour is also presented, which is a typical transonic flow field.

The iso-surfaces with one variable being constant are illustrated in Fig. 8. It can be seen that all parameters besides the angle of attack, including span, sweep angle, and root chord length, have significant effects on the optimization objective near the optimum solution. The contribution of each geometric design variable to the lift-to-drag ratios is displayed with a percentage in Fig. 9 based on the parameter sensitivity analysis. Different from the subsonic case, the most contribution to the lift-to-drag ratios in the transonic case come from the span with 84% and the sweep angle and root chord length are secondary with similar effects.

3.2.3 $Ma_\infty = 2.0$ and $H = 300$ m

At the supersonic case, the range of design variables is shown in Table 7 in terms of a pre-optimization result. The computational domain is smaller than the preceding two cases due to the supersonic computation, in which the upstream distance from the model nose is 5 times the body length, the downstream is 10 times the body length from the model bottom, and the side is 10 times the body length from the symmetry plane. Total grid cells are around 1.4 million, and will vary

**Fig. 7** Optimum configuration at $Ma = 0.85$. **a** optimum configuration and grid; **b** pressure distribution

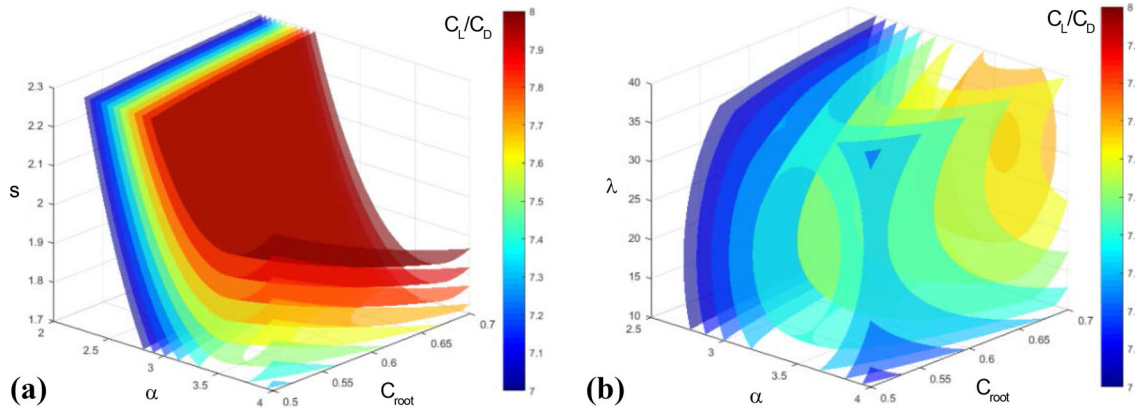


Fig. 8 Iso-surfaces of response surface at $Ma = 0.85$. **a** C_L/C_D v.s. α , c_{root} and s with $\lambda = 32.1$ deg; **b** C_L/C_D v.s. α , c_{root} , and λ with $s = 1.7$ m

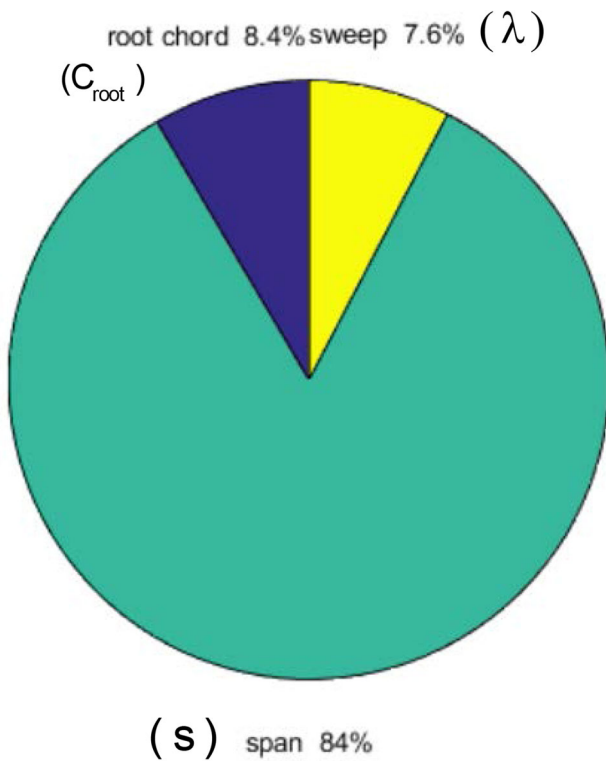


Fig. 9 Global sensitivity results of design variables at $Ma = 0.85$

slightly with the re-meshing during the optimization. The grid amount is sufficient in terms of the preceding grid convergence testing. The surrogate models at this case based on 180 data points are employed, which is obtained by invoking the CFD solver and friction drag estimation code repeatedly. The fitting accuracy of the surrogate models was estimated with a R^2 value of 0.98, indicating that the fitting accuracy is good.

Table 7 Range of design variables at $Ma_\infty = 2.0$

Design variables	α /deg	C_{root}	λ /deg	s /m
Lower bound	0.3	1.8	65.0	0.6
Upper bound	1.1	2.2	74.0	0.7

Table 8 Optimization result at $Ma_\infty = 2.0$

Models	α /deg	C_{root}	λ /deg	s /m	C_L	$\partial C_M / \partial C_L$	C_L / C_D
RSM	1.06	1.83	69.3	0.62	0.038	-0.042	0.45
Kriging	1.03	1.83	70.1	0.62	0.038	-0.041	0.45

The optimization result is shown in Table 8, and the associated optimum configuration and flow field are illustrated in Fig. 10, in which the configuration at the supersonic condition has a high sweep and low aspect ratio wing that is greatly different from the preceding two cases. The optimum parameters consist of sweep angle of 70.1° and span of 0.62 m, and root chord length of 1.83 m. The wing with a high-sweep angle and low aspect ratio has better aerodynamic characteristics at supersonic speeds. The optimum configuration also satisfies static stability and lift coefficient constraints. The pressure distribution in Fig. 10b shows a typical supersonic flow field.

The iso-surfaces with one variable being constant are illustrated in Fig. 11. All parameters, besides the angle of attack, including span, sweep angle, and root chord length, have effects on the optimization objective near the optimum solution. The sensitivity analysis in Fig. 12 quantitatively characterizes the contributions of each geometric design variable to the lift-to-drag ratios. Most of the contribution came from the span with 65% and the root chord length and sweep angle account for 26.4% and 86%, respectively.

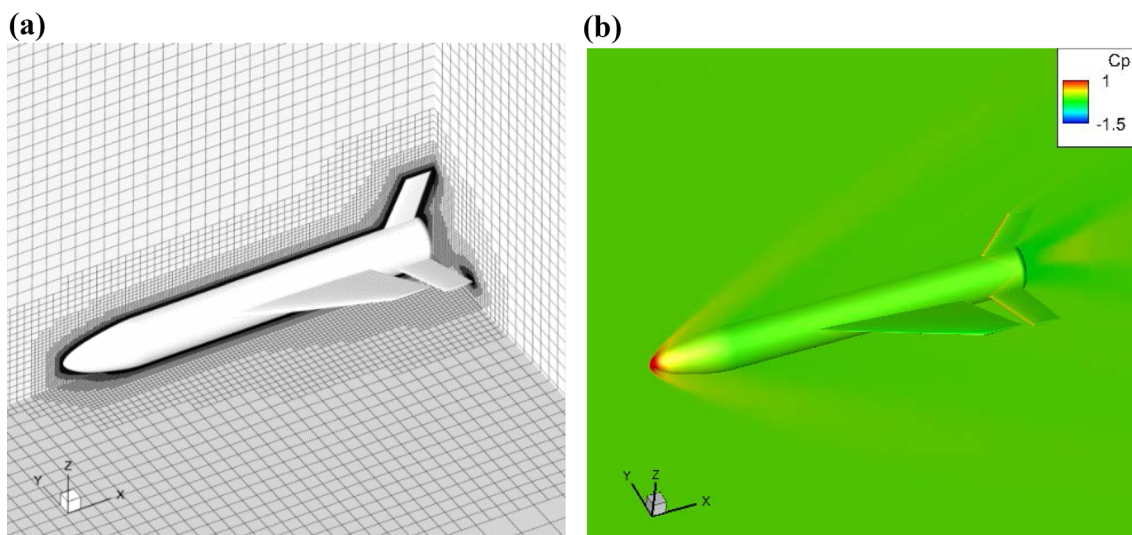


Fig. 10 Optimum configuration at $Ma = 2.0$. **a** Optimum configuration and grid; **b** pressure distribution

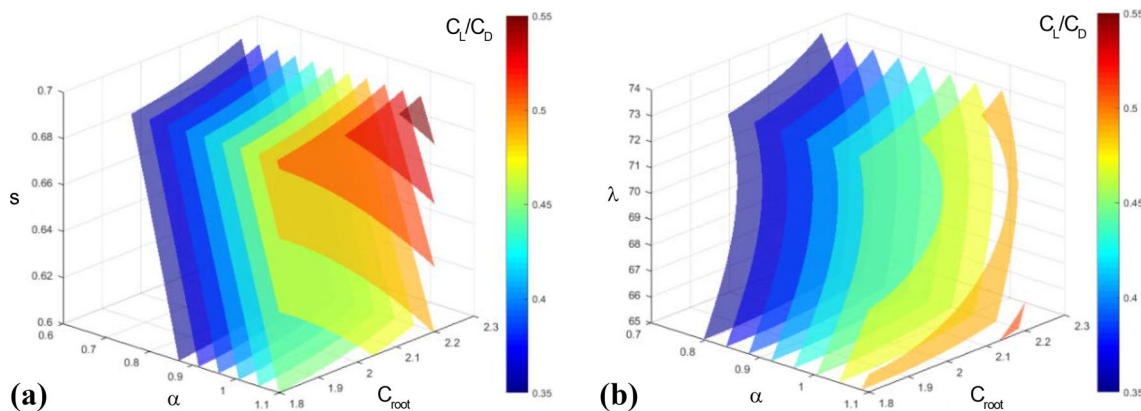


Fig. 11 Iso-surface presentation of response surface at $Ma = 2.0$. **a** C_L/C_D v.s. α , C_{root} and s with $\lambda = 71.3$ deg; **b** C_L/C_D v.s. α , C_{root} , and λ with $s = 0.6$ m

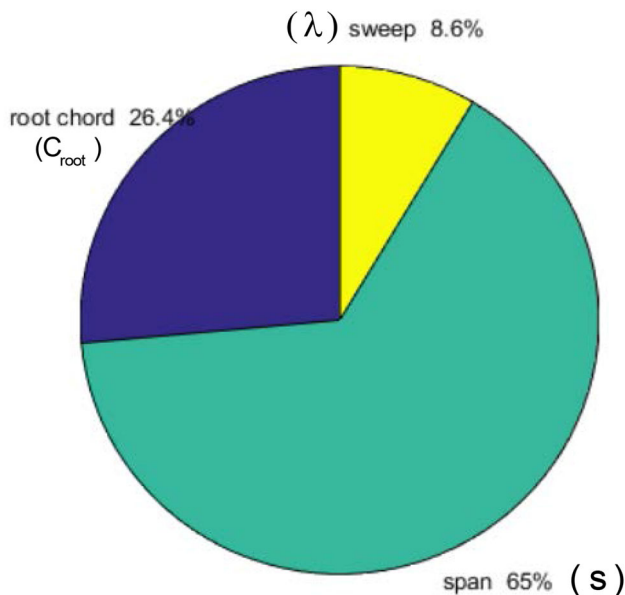


Fig. 12 Global sensitivity results of design variables at $Ma = 2.0$

3.2.4 Aerodynamic Characteristics at Off-design Points

Figure 13a shows the lift-to-drag ratios at various AOAs for three design Mach numbers to demonstrate the aerodynamic characteristics at off-design points, in which the C_L/C_D of each optimal configuration is marked by a small circle. In the subsonic case ($Ma = 0.5$), the maximum value of C_L/C_D is the lift-to-drag ratio of the optimal configuration, but for the transonic ($Ma = 0.85$) or supersonic case ($Ma = 2.0$), the optimized C_L/C_D is not the maximum one due to the limitation of lift constraints (see Tables 1 and 2). The weight of the aircraft is given in each flight condition, so the lift coefficient as a constraint is fixed in a small range during the optimization (Table 1). Figure 13b presents the lift coefficients against AOAs, and the optimal AOA is also marked by small circles for each Ma . The optimal lift coefficients for $Ma = 0.85$ and 2.0 all reach the upper limits of the constraints (Table 1), which restricts the further increase of lift-to-drag ratios. In addition, note that conventional aerodynamic optimization

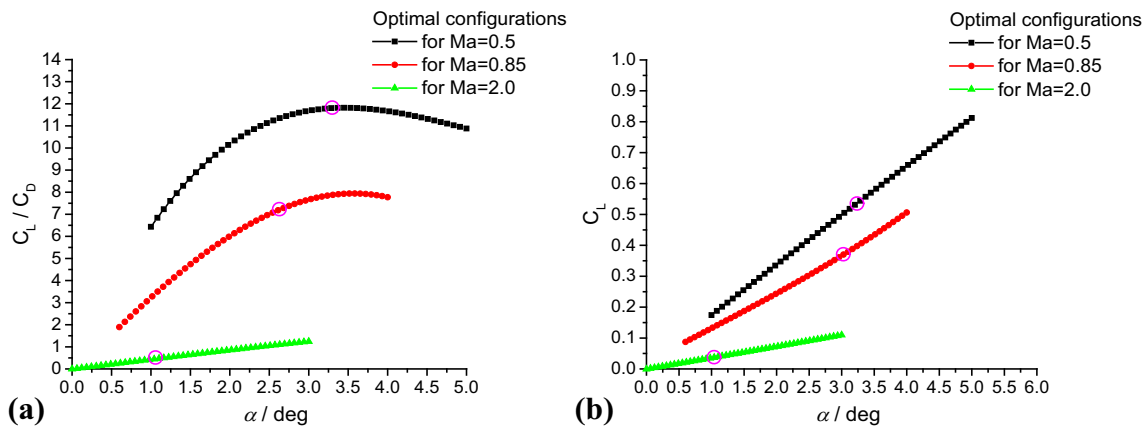


Fig. 13 Variation of **a** lift-to-drag ratio C_L/C_D and **b** lift coefficient C_L with AOAs

is commonly based on a base configuration, around which small geometric modifications are imposed in optimization, but the morphing aircraft can tailor their configurations to an optimum one at each flight condition, therefore generally no base configurations exist.

4 Summary and Conclusions

The optimum configurations were determined for a morphing-wing aircraft with variable sweep, span, and chord length using an aerodynamic optimization study at subsonic, transonic and supersonic conditions. The objective of the optimization is to obtain maximum lift-to-drag ratios subject to lift coefficients and static stability at each flight condition. A surrogate model approach based on response surfaces and Kriging models was employed in optimization to reduce the computational cost, and the optimizer with a genetic algorithm searches the optimum solution in the entire design space. The aerodynamic forces are calculated by an Euler-based solver and friction drag estimation code. Besides the optimum configuration corresponding to any flight condition being obtained, a global sensitivity analysis based on the response surface model was also carried out, therefore the contribution of each design variable to the optimization objective was analyzed. The results indicated that the optimum configuration at subsonic speeds has a lower sweep wing with high aspect ratio, and the wing sweep has a primary contribution to lift-to-drag ratios, and the span is secondary; at transonic conditions, however, the medium-sweep wing is the optimum, and the contribution of the span is far more than other design variables; at supersonic conditions, the optimum wing becomes a high-sweep cropped delta wing, and the span has a dominant contribution to lift-to-drag ratios, and the sweep angle is secondary.

References

- Weisshaar TA (2013) Morphing aircraft systems: historical perspectives and future challenges. *J Aircr* 50(2):337–353
- Vasista S, Tong L, Wong KC (2012) Realization of morphing wings: a multidisciplinary challenge. *J Aircr* 49(1):11–28
- Ajaj RM, Beaverstock CS, Friswell MI (2016) Morphing aircraft: the need for a new design philosophy. *Aerosp Sci Technol* 49(4):154–166
- Youda Ye (2009) Study on aerodynamic characteristics and design optimization for high speed near space vehicles. *Adv Mech* 39(6):683–694
- Xuzhao He, Zheng Zhou, Si Qin, Feng Wei, Jialing Le (2016) Design and experimental study of a practical Osculating Inward Cone Waverider Inlet. *Chin J Aeronaut* 29(6):1582–1590
- Hicken JE, Zingg DW (2010) Induced-drag minimization of nonplanar geometries based on the euler equations. *AIAA J* 48(11):2564–2575
- Gagnon H, Zingg DW (2016) Euler-equation-based drag minimization of unconventional aircraft configurations. *J Aircr* 53(5):1361–1371
- Kenway GW, Martins JRRA (2016) Multipoint aerodynamic shape optimization investigations of the common research model wing. *AIAA J* 54(1):113–128
- Lyu Z, Kenway GW, Martins JRRA (2015) Aerodynamic shape optimization investigations of the common research model wing benchmark. *AIAA J* 53(4):968–985
- Fincham JHS, Friswell MI (2015) Aerodynamic optimisation of a camber morphing aerofoil. *Aerosp Sci Technol* 43:245–255
- Secanell M, Suleman A, Gamboa P (2006) Design of a morphing airfoil using aerodynamic shape optimization. *AIAA J* 44(7):1550–1562
- Namgoong H, Crossley WA, Lyrintzis AS (2007) Aerodynamic optimization of a morphing airfoil using energy as an objective. *AIAA J* 45(9):2113–2124
- Gamboa P, Vale J, Lau FJP, Suleman A (2009) Optimization of a morphing wing based on coupled aerodynamic and structural constraints. *AIAA J* 47(9):2087–2104
- Spearman ML (2012) Aerodynamic research at NACA/NASA langley related to the use of variable-sweep wings. In: 50th AIAA aerospace sciences meeting including the new horizons forum and aerospace exposition 09–12 January 2012, Nashville, Tennessee, AIAA Paper 2012–0956

15. Bae J-S, Seigler TM, Inman DJ (2005) Aerodynamic and static aeroelastic characteristics of a variable-span morphing wing. *J Aircr* 42(2):528–534
16. Mestrinho J, Gamboa P, Santos P (2011) Design optimization of a variable-span morphing wing for a small UAV. In: 52nd AIAA/ASME/ASCE/AHS/ASC structures, structural dynamics and materials conference 19th 4–7 April 2011, Denver, Colorado, AIAA Paper 2011–2025
17. Ajaj RM, Friswell MI, Saavedra Flores EI, Little O, Isikveren AT (2012) Span morphing: a conceptual design study. In: 53rd AIAA/ASME/ASCE/AHS/ASC structures, structural dynamics and materials conference 20th AI 23–26 April 2012, Honolulu, Hawaii, AIAA Paper 2012–1510
18. Woods BKS, Friswell MI (2016) The adaptive aspect ratio morphing wing: design concept and low fidelity skin optimization. *Aerosp Sci Technol* 42:209–217
19. Ismail NI, Zulkifli AH, Abdullah MZ, Hisyam Basri M, Norazharuddin Shah A (2014) Optimization of aerodynamic efficiency for twist morphing MAV wing. *Chin J Aeronaut* 27(3):475–487
20. Hunsaker DF, Phillips WF and Joo JJ (2017) Aerodynamic shape optimization of morphing wings at multiple flight conditions. In: AIAA scitech forum, 9–13 January 2017, Grapevine, Texas, 55th AIAA aerospace sciences meeting, AIAA Paper 2017–1420
21. Su WH, Swei SS-M, Zhu GG (2016) Optimum wing shape of highly flexible morphing aircraft for improved flight performance. *J Aircr* 53(5):1–12
22. Queipo NV, Haftka RT, Shyy W, Goel T, Vaidyanathan R, Tucker PK (2005) Surrogate-based analysis and optimization. *Prog Aerosp Sci* 41:1–28
23. Forrester AIJ, Keane AJ (2009) Recent advances in surrogate-based optimization. *Prog Aerosp Sci* 45:50–79
24. McDonald R Open VSP. www.openvsp.org. Accessed 1 Mar 2017
25. McDonald RA (2015) Interactive reconstruction of 3D models in the openVSP parametric geometry tool. In: 53rd AIAA aerospace sciences meeting, AIAA SciTech Forum, AIAA 2015–1014, 2015
26. Aftosmis MJ Cart3D Resource Website. <http://people.nas.nasa.gov/aftosmis/cart3d/cart3Dhome.html>. Accessed 1 Mar 2017
27. Nemec M, Aftosmis MJ, Pulliam TH (2004) CAD-based aerodynamic design of complex configurations using a cartesian method. In: 42nd AIAA aerospace sciences meeting, 2004, AIAA Paper 2004–0113
28. Ordaz I, Li W (2014) Integration of off-track sonic boom analysis in conceptual design of supersonic aircraft. *J Aircr* 51(1):23–28
29. Ordaz I, Geiselhart KA, Fenbert JW (2015) Conceptual design of low-boom aircraft with flight trim requirement. *J Aircr* 52(3):932–939
30. Gur O, Mason WH, Schetz JA (2010) Full configuration drag estimation. *J Aircr* 47(4):110–116
31. Saltelli A, Sobol IM (1995) Sensitivity analysis for nonlinear mathematical models: numerical experience. *Math Models Comput Exp* 7(11):16–28
32. Cannavó Flavio (2012) Sensitivity analysis for volcanic source modeling quality assessment and model selection. *Comput Geosci* 44:52–59
33. Changli Hu, Wang Guoyu, Chen Guanghao, Huang Biao (2015) Surrogate model-based optimization for the headform design of an axisymmetric body. *Ocean Eng* 107:237–245
34. The 2nd AIAA CFD Drag Prediction Workshop. <https://aiaa-dpw.larc.nasa.gov/Workshop2/workshop2.html>. [Retrieved March 2017]
35. Sahu J, Heavey KR (2009) Computations of supersonic flow over a complex elliptical missile configuration. In: AIAA Atmospheric flight mechanics conference 10–13 August 2009, Chicago, Illinois, AIAA Paper 2009–5714